Confinement of MgH_2 Nanoclusters within Nanoporous Aerogel Scaffold Materials

Thomas K. Nielsen,[†] Kandavel Manickam,[‡] Michael Hirscher,[‡] Flemming Besenbacher,[†] and Torben R. Jensen[†,*]

[†]Interdisciplinary Nanoscience Center (iNANO) and Department of Chemistry, Aarhus University, DK-8000 C Aarhus, Denmark, and [‡]Max-Planck-Institut für Metallforschung, Heisenbergstrasse 3, D-70569 Stuttgart, Germany

ABSTRACT Nanoparticles of magnesium hydride were embedded in nanoporous carbon aerogel scaffold materials in order to explore the kinetic properties of hydrogen uptake and release. A new modified procedure for the synthesis of magnesium hydride nanoparticles is presented. The procedure makes use of monoliths (~0.4 cm^3) of two distinct types of nanoporous resorcinol–formaldehyde carbon aerogels loaded with dibutylmagnesium, $MgBu_2$. Excess $MgBu_2$ was removed mechanically, and the increase in mass was used as a measure of the amount of embedded MgH_2. Energy-dispersive spectrometry revealed that MgH_2 was uniformly distributed within the aerogel material. *In situ* synchrotron radiation powder X-ray diffraction showed that $MgBu_2$ transformed directly to MgH_2 at $T \sim 137$ °C and $p(H_2) = 50$ bar. Two distinct aerogel samples, denoted X1 and X2, with pore volumes of 1.27 and 0.65 mL/g and average pore sizes of 22 and 7 nm, respectively, were selected. In these samples, the uptake of magnesium hydride was found to be proportional to the pore volume, and aerogels X1 and X2 incorporated 18.2 and 10.0 wt % of MgH_2, respectively. For the two samples, the volumetric MgH_2 uptake was similar, ~12 vol %. The hydrogen storage properties of nanoconfined MgH_2 were studied by Sieverts' measurements and thermal desorption spectroscopy, which clearly demonstrated that the dehydrogenation kinetics of the confined hydride depends on the pore size distribution of the scaffold material; that is, smaller pores mediated faster desorption rates possibly due to a size reduction of the confined magnesium hydride.

KEYWORDS: nanoconfinement · nanoporous scaffold · carbon aerogel · magnesium hydride · hydrogen storage

Hydrogen has been suggested as a future carrier of renewable energy, but a compact, efficient, robust, safe, and inexpensive hydrogen storage system remains to be developed.[1,2] Hydrogen storage in the solid state appears to have the greatest potential to fulfill all of these requirements, in particular, for mobile applications, and therefore, a breakthrough in this research area calls upon the synthesis of new nanostructured materials.[3−5] In the past, magnesium and Mg-based alloys have been explored intensively due to the high theoretical gravimetric H_2 density in magnesium hydride, MgH_2, $\rho_m = 7.6$ wt %, and the high volumetric H_2 density, $\rho_v = 110$ g/L. Magnesium is also a cheap and abundant metal, making it suitable for large-scale hydrogen storage applications. Unfortunately, the use of magnesium hydride is hampered by relatively slow kinetics for hydrogen release and uptake, and also the thermodynamics, $\Delta H_f = -75$ kJ/mol H_2, is rather unfavorable (*i.e.*, MgH_2 must be heated to *ca.* 300 °C in order to release hydrogen at $p(H_2) = 1$ bar).[1,6] Nanoscience may provide novel ideas and solutions to these issues, as suggested in this study. Several factors hinder the rate of hydrogenation and dehydrogenation of the Mg/MgH_2 system. The surface oxide layer, which surrounds the magnesium metal, decreases the kinetics significantly because this phase is almost impermeable to hydrogen.[7] Another obstacle is the slow diffusivity of hydrogen in MgH_2; the diffusion constant of hydrogen atoms is much smaller in MgH_2 as compared to Mg. The initial MgH_2 formation therefore occurs as a fast process, but a shell of the near surface hydride eventually encloses the metal and significantly decreases the hydrogen kinetics. This obstacle also reduces the reversible hydrogen storage capacity upon cycling H_2 release and uptake.[8−11]

These inherent problems may be solved by utilizing magnesium nanoclusters for hydrogen storage because the nanosize of Mg induces several advantages: (i) reduction of diffusion distances enhances the rate at which hydrogen is distributed and decreases the influence of the oxide and/or hydride surface layer;[8,12−14] (ii) an increased surface area to bulk volume ratio favors hydrogen bond dissociation; and (iii) an increased ratio of hydrogen atoms in the grain boundary also enhances the hydrogen diffusion rates.[12,15,16] These properties all help to improve the hydrogenation/dehydrogenation kinetics of magnesium, and also the thermodynamics is improved.

*Address correspondence to trj@chem.au.dk.

Received for review August 24, 2009 and accepted October 22, 2009.

Published online November 2, 2009.
10.1021/nn901072w CCC: $40.75

The increased surface area to bulk volume ratio destabilizes MgH_2 and thereby reduces the reaction enthalpy as described in recent theoretical studies.[17−20] However, these kinetic and thermodynamic improvements are found to depend significantly on the size of the Mg nanoclusters. Thermodynamic improvements are suggested to occur only for small nanoparticles with a size less than 2−5 nm, while the kinetics is enhanced also for larger nanoparticles up to ~30−50 nm.[8,12,20] Unfortunately, nanoparticles of, for example, metal hydrides tend to agglomerate and grow into larger particles upon hydrogen release and uptake cycles.[12,21−23] Consequently, there is an urgent need for development of novel nanoconfinement systems which can prohibit agglomeration and grain growth and which are stable over many hydrogen release and uptake cycles. One approach is to introduce the hydride into a porous inert scaffold material. In this way, the size of the metal hydride is determined by the pore size distribution of the scaffold, and particle growth will be hindered by the compartmentalization within the respective pores. This principle has already been applied to a number of promising hydrogen storage materials. Ammonia borane (NH_3BH_3) was incorporated into a mesoporous silica scaffold, which led to an increase in the hydrogen desorption kinetics and thermodynamic improvements relative to that of bulk samples.[24] Faster desorption rates for $NaAlH_4$ nanoparticles loaded into porous scaffold materials have also been reported.[25] Furthermore, it was recently demonstrated that the hydrogen desorption kinetics of $LiBH_4$ increased when introduced into nanoporous scaffolds.[26] Carbon-supported magnesium nanoparticles have been prepared by melt infiltration,[27,28] but recently, a new method has been suggested. MgH_2 was loaded into a carbon aerogel material with an average pore size of 13 nm by means of an organic precursor, dibutylmagnesium ($MgBu_2$), which resulted in an improvement of the hydrogen desorption kinetics as compared to ball milled samples.[29]

The previously applied method for synthesis of nanoconfined magnesium hydride is here modified by utilizing carbon aerogel monoliths with a potential to increase the fraction of nanoconfined magnesium hydride in the composite material relative to hydride deposited on the aerogel surface.[29] Furthermore, opposed to previous studies, the focus of this work is to demonstrate that the properties of confined MgH_2 nanoparticles can, in fact, be tailored by varying the texture parameters of the porous scaffold material. We have prepared samples of magnesium hydride nanoparticles incorporated into scaffold materials with different porosity and studied the uptake of MgH_2 and the hydrogen storage properties hereof. Resorcinol formaldehyde carbon aerogels (RF-gels) utilized here are inert and stable under the conditions used for cycling hydrogen release and uptake in magnesium hydride and can be prepared as large monoliths. Furthermore, the pore size distribution of these gels can be tuned by varying the synthetic conditions.[30,31]

TABLE 1. Texture Parameters for the Aerogel Scaffold Materials

RF-aerogel	S_{BET} (m^2/g)	V_{meso} (mL/g)	V_{tot} (mL/g)	V_{micro}/V_{total}	D_{max} (nm)
X1	723	1.1	1.27	0.15	22
X2	686	0.5	0.65	0.24	7

RESULTS AND DISCUSSION

Nanoporous Scaffold Materials. Two aerogel scaffold materials were selected for this study, and their texture parameters are given in Table 1. The values are in good agreement with previous results for materials prepared under similar conditions.[26,30] The two aerogel scaffolds are considerably different with respect to the total volume and the pore size distribution. Aerogel X1 has twice the total volume per unit mass, V_{tot}, as compared to aerogel X2, and the average pore size is three times as large (see D_{max}). In contrast, the BET surface areas of the gels are similar.

To ensure that the MgH_2 nanoparticles are not only deposited onto the surface of the scaffold materials, we used monoliths of aerogels (~0.4 cm^3) for this study with the advantage that excess surface precipitated white crystalline dibutylmagnesium ($MgBu_2$) can easily be removed mechanically from the black aerogel monoliths. In the following, samples of aerogels X1 and X2 loaded with MgH_2 are referred to as X1-Mg and X2-Mg, respectively.

Magnesium Hydride Nanoparticles. The two aerogel samples X1 and X2 were placed in dibutylmagnesium heptan solution and absorbed $MgBu_2$. The amount of nanoconfined $MgBu_2$ can conveniently be calculated from the weight gain of aerogel monoliths measured after drying for several days and after mechanical removal of surface excess $MgBu_2$. The amount of nanoconfined magnesium hydride in aerogels X1 and X2 can be calculated stoichiometrically from the amount of $MgBu_2$ and corresponds to 18.2 and 10.0 wt % MgH_2, respectively. The volume of nanoconfined magnesium hydride per unit mass of sample can be calculated using the bulk density of magnesium hydride, $\rho = 1.45$ g/mL. The volumetric amount of nanoconfined magnesium hydride can be found dividing with the total pore volume of the aerogel, V_{tot}. The difference in MgH_2 content compares well to the difference in V_{tot} of the respective aerogel samples, as revealed from Tables 1 and 2.

The synthesis of MgH_2 from crystalline dibutylmagnesium embedded in the aerogel monoliths was studied by *in situ* synchrotron radiation powder X-ray diffraction, SR-PXD (see Figure 1).

Diffraction from crystalline dibutylmagnesium is visible in the temperature range from room temperature to 137 °C. The direct conversion of $MgBu_2$

TABLE 2. MgH_2 Content and Hydrogen Release from the Aerogel Materials[a]

sample	MgH_2[a] (wt %)	MgH_2[b] (vol %)	H_2[a] (wt %)	H_2[c] (wt %)	H_2[d] (wt %)
X1-Mg	18.2	12.1	1.40	1.45	1.14
X2-Mg	10.0	11.7	0.76	1.12	0.62

[a]Calculated from the uptake of dibutylmagnesium. [b]Calculated from the uptake of dibutylmagnesium using bulk density of MgH_2. [c]Measured by the Sieverts' method, desorption cycle 1. [d]Measured by the Sieverts' method, desorption cycle 4.

into MgH_2 occurred within a few minutes according to reaction scheme 1, and the reaction is completed at $T = 157$ °C.

$$Mg(C_4H_9)_2(s) + 2H_2(g) \rightarrow MgH_2(s) + 2C_4H_{10}(g) \quad (1)$$

There are no indications of chemical reactions between the aerogel scaffold material and MgH_2 or Mg. Similar results were obtained for sample X2-Mg. A sample of MgH_2, denoted AM, was prepared under similar conditions by precipitation from a dibutylmagnesium heptan solution without the presence of aerogel. Powder X-ray diffraction (PXD) diagrams of samples AM and X1-Mg before and after the synthesis of MgH_2 are compared in Figure 2.

The position of reflections from pure $MgBu_2$ and $MgBu_2$ loaded into the RF-gel coincides well. As opposed to the PXD diagrams of samples $MgBu_2$ and AM, broad reflections at $2\theta \sim 13.8$ and 25.4° are observed in the diagrams of samples X1-$MgBu_2$ and X1-Mg, indicating X-ray diffraction from the RF-gel. The broad reflections are due to graphite-like structural features within the gel, which is in agreement with previous studies.[32]

Several hydrogen release and uptake cycles of magnesium hydride nanoparticles within the aerogels were studied by a Sieverts' apparatus (see Figures 3−5) and subsequently by scanning electron microscopy, SEM, and energy-dispersive spectrometry, EDS (see Figures S1−S6 in the Supporting Information). The X2-Mg samples appear more condensed as compared to

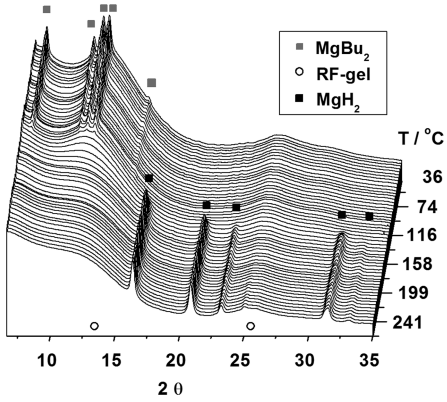

Figure 1. Selected part of *in situ* SR-PXD data showing the synthesis of MgH_2 from dibutylmagnesium ($MgBu_2$) within sample X1-Mg. The sample was heated from room temperature to 350 °C (heating rate 7.5 °C/min) under a hydrogen pressure of $p(H_2) = 50$ bar ($\lambda = 0.9077$ Å).

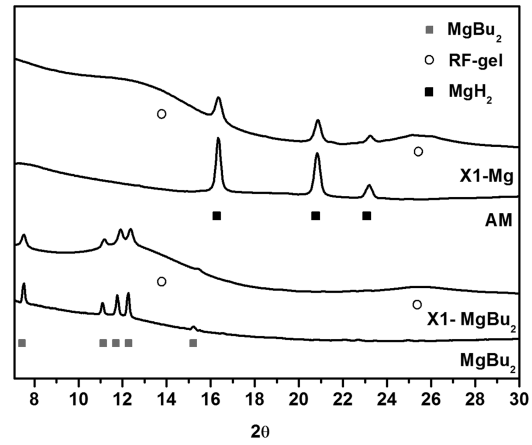

Figure 2. Synchrotron radiation powder X-ray diffraction diagrams measured at room temperature for samples AM and X1-Mg before and after the synthesis of MgH_2. The diagrams were normalized individually with regard to the most intensive reflection from $MgBu_2$ or MgH_2 ($\lambda = 0.9077$ Å).

sample X1-Mg by SEM images (see Figures S1 and S4), which is expected from the D_{max} and V_{tot} values given in Table 1. The EDS element analysis (Figures S2 and S5) discloses the presence of magnesium, carbon, oxygen, and a small amount of aluminum in samples X1-Mg and X2-Mg. Oxygen is present as a part of the aerogel structure,[31] but oxygen also originates from the oxidation of magnesium due to the exposure to ambient conditions prior to analysis. The aluminum impurity originates from the dibutylmagnesium solution which also contains triethylaluminum. According to earlier studies, small amounts of aluminum are not expected to have any catalytic effect on the hydrogenation and dehydrogenation of magnesium but may influence kinetics by formation of Mg−Al alloys.[33] EDS maps are shown in Figures S3 and S6 and illustrate that magnesium is uniformly distributed as nanoparticles throughout both aerogel scaffolds.

Kinetic Properties of the Nanoconfined MgH_2. Figure 3 displays the hydrogen desorption curves (nos. 1 and 4) for sample X1-Mg as measured by a Sieverts' apparatus.

During the first cycle, sample X1-Mg desorbs 1.45 wt % H_2, which is above the theoretical value of 1.40

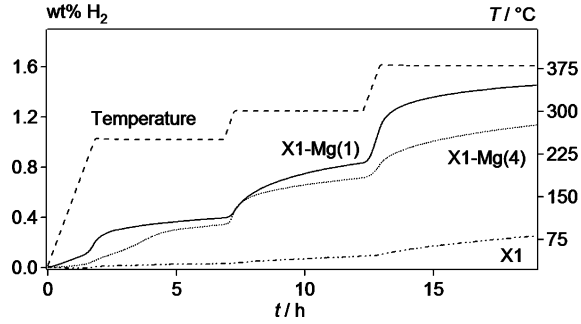

Figure 3. Sieverts' measurement of hydrogen desorption cycles 1 and 4 for sample X1-Mg (solid and dotted lines, respectively) and the first desorption cycle for "empty" aerogel X1 (dash-dotted line) performed at fixed temperatures of 250, 300, and 380 °C (heating rate 2 °C/min; see the dashed line).

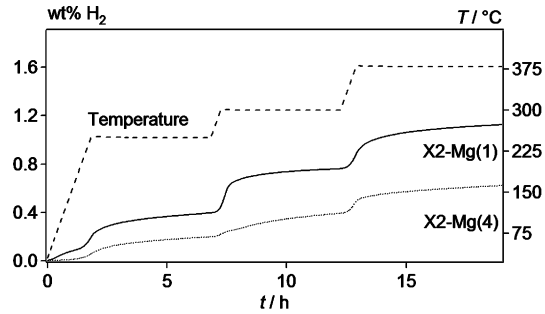

Figure 4. Sieverts' measurement of hydrogen desorption cycles 1 and 4 for sample X2-Mg (solid and dotted lines, respectively) performed at fixed temperatures of 250, 300, and 380 °C (heating rate 2 °C/min; see the dashed curve).

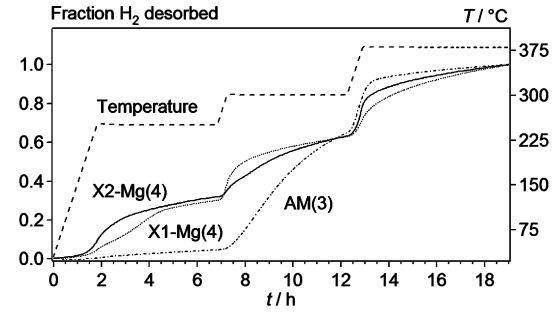

Figure 5. Sieverts' measurement of desorption profiles for samples X1-Mg, X2-Mg, and AM (dotted, solid, and dash-dotted lines, respectively) performed at fixed temperatures of 250, 300, and 380 °C (heating rate 2 °C/min). Data are normalized and show the fraction of released hydrogen.

wt % H_2 (see Table 2), and the onset temperature is unrealistically low, $T_{onset} \sim 55$ °C. This indicates that gases other than hydrogen are released during the first desorption cycle. The excess gas released at lower temperatures may be butane residing in the partly hydrogenated $MgBu_2$ particles. $MgBu_2$ may be covered by a layer of MgH_2, which retards the hydrogenation further. Desorption profile data for aerogel X1 without magnesium hydride confined in the pores were measured as a reference standard (see Figure 3). Gaseous compounds are released from the scaffold material at temperatures above 250 °C, and the molar quantity of the gas released from the empty aerogel sample corresponds to 0.25 wt % H_2. The onset temperature for gas release during the fourth desorption cycle is at ~210 °C, and an amount of gas equivalent to 1.14 wt % H_2 is desorbed, which indicates that only hydrogen is liberated.

Sample X2-Mg shows the same characteristics for hydrogen desorption (see Figure 4) as was observed for sample X1-Mg (see Figure 3). Aerogel X2 is twice as condensed as aerogel X1, as seen from V_{tot} given in Table 1, and the release of excess gases therefore influences the first desorption cycle of sample X2-Mg to a greater extent, as depicted in Figures 3 and 4. Otherwise, the same trends apply to sample X2-Mg, where 0.62 wt % H_2 is released during the fourth desorption cycle. For both samples, approximately 81% of the theoretical hydrogen content is released during the fourth desorption cycle. The fact that the measured hydrogen capacity of sample X1-Mg is approximately twice the value of sample X2-Mg coincides well with the uptake of MgH_2 in aerogels X1 and X2, which is 18.2 and 10.0 wt %, respectively. Furthermore, the relative content of magnesium hydride and hydrogen within the respective aerogel materials is in good agreement with the individual pore volumes (see Table 1). The volumetric magnesium hydride content in the aerogels was calculated using the bulk density of MgH_2. The calculations reveal that MgH_2 occupies ~12 vol % of the total pore volume, V_{tot}, in both aerogel scaffold materials. The excess gases released from the scaffold materials influenced the measurements during the first two cycles for sample X1-Mg and the first three cycles for sample X2-Mg.

Normalized desorption profiles of samples AM, X1-Mg, and X2-Mg are compared in Figure 5. Samples X1-Mg and X2-Mg release ~30% of the hydrogen content at $T \leq 250$ °C. In contrast, sample AM only releases ~5% of the hydrogen content at $T \leq 250$ °C. In addition, sample X2-Mg has a significantly faster desorption rate at low temperatures, in particular, during the first 3 h of measurement. This finding shows that the hydrogen desorption kinetics is improved considerably when magnesium hydride is present as nanoparticles in the nanoporous aerogel scaffold materials as compared to the nonconfined sample. It is noteworthy that the smaller the pores in the scaffold material, the larger is the improvement of the desorption kinetics at low temperatures. This suggests that the difference in hydrogen desorption kinetics of the samples in Figure 5 is due to different average size of the imbedded MgH_2 nanoparticles.

The results discussed above were based on Sieverts' measurements in which pressure changes were detected (*i.e.*, amount of hydrogen gas molecules). In order to measure hydrogen release selectively, the kinetics of the first desorption cycle within the respective gels was studied by thermal desorption spectroscopy (TDS) (see Figure 6), in which case the release of hydrogen was detected by a mass spectrometer. Bulk micrometer-sized MgH_2, denoted BM, and sample AM were used as reference.

The characteristic parameter extracted from TDS measurements is the temperature T_{max}, where the desorption rate reaches its maximum value and also the onset temperature T_{onset} for release of hydrogen. From these parameters, the kinetic properties of each sample can be compared qualitatively. The appearance of several maxima on the desorption curve suggests several desorption processes with different kinetic properties.

The bulk micrometer-sized (BM) and the as-synthesized (AM) MgH_2 samples have T_{max} values of 515 and 406 °C, respectively. This difference may be regarded as a size-mediated effect because the direct syn-

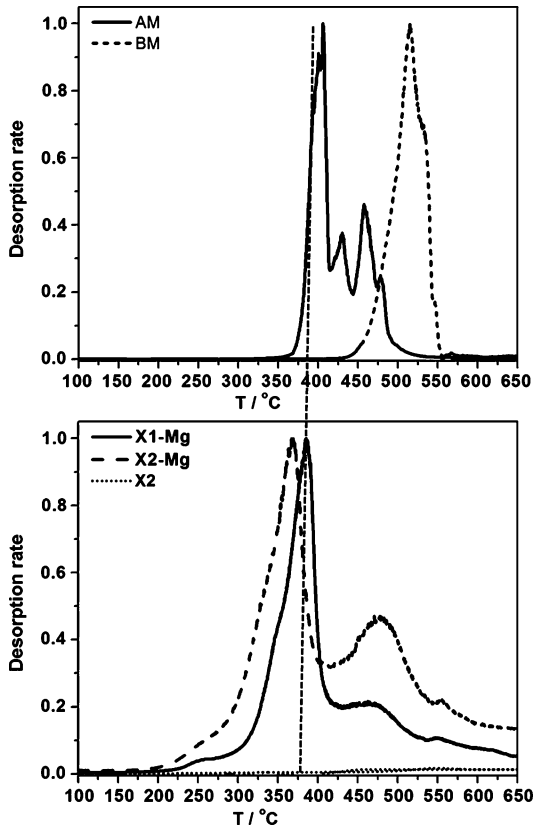

Figure 6. Normalized thermal desorption spectroscopy profiles measured from room temperature to 700 °C (heating rate 3.6 °C/min) by recording the mass spectrometer intensity of H_2^+ ions ($m/e = 2$). Upper graph shows hydrogen desorption from magnesium hydride prepared from dibutylmagnesium (AM) compared to bulk magnesium hydride (BM). The lower graph compares the two aerogel—magnesiumhydride samples X1-Mg and X2-Mg and the "empty" aerogel X2.

thesis of MgH_2 from dibutylmagnesium (AM) may result in a smaller average grain size distribution as compared to the conventional MgH_2 sample. A significantly thinner surface oxide layer is also expected for the freshly prepared sample of MgH_2 (AM). Notice, in this study, there is no indication of the presence of any magnesium oxide in the X-ray diffraction data. The desorption profile of the AM sample shows two additional local T_{max} values at 430 and 456 °C, respectively, indicating different crystal sizes within the sample. The TDS measurements were also carried out for virgin aerogels with no MgH_2 nanoparticles using the same conditions, in which case the TDS signal is approximately 2 orders of magnitude lower. This shows that practically no hydrogen gas is released from pure RF-gel (see Figure 6).

Samples X1-Mg and X2-Mg have TDS T_{max} values of 385 and 367 °C, respectively, and T_{onset} values of 200 and 175 °C, demonstrating that the hydrogen desorption occurs at lower temperatures due to the decreasing pore size of the scaffold materials. Furthermore, the kinetics of hydrogen release from nanosized MgH_2 (X2-Mg) is significantly improved as compared to MgH_2 freshly prepared from $MgBu_2$. This is evident from the T_{max} and T_{onset} values, which have been reduced by 39 and 175 K, respectively (see Table 3). The kinetic enhancement of hydrogen released from the nanosized MgH_2 (X2-Mg) is even more evident relative to the conventional micrometer-sized MgH_2 (BM) since the T_{max} and T_{onset} values are decreased by 148 and 260 K, respectively.

TABLE 3. Accumulated Hydrogen Desorbed below Selected Temperatures of 325, 375, 425, and 700 °C (The Temperature for the Onset of Hydrogen Release, T_{onset}, and Maximum of the Release Rate, T_{max}, Is Also Provided)

sample	<325 °C	<375 °C	<425 °C	<700 °C	T_{onset}/°C	T_{max}/°C
X2-Mg	13.3%	39.0%	53.8%	100%	175	368
X1-Mg	8.1%	33.9%	64.8%	100%	200	385
AM	0.8%	1.9%	56.2%	100%	350	406
BM	0.3%	0.4%	0.6%	100%	435	515

In Table 3, the samples are compared with regard to the accumulated amount of desorbed hydrogen at selected temperatures. It is evident that magnesium hydride nanoparticles within the aerogel scaffold materials desorb a larger fraction of the total hydrogen content at lower temperatures as compared to the bulk MgH_2 samples, but also when the average pore size of the aerogel decreases accordingly. Samples X1-Mg and X2-Mg have local T_{max} values at 466 and 477 °C, respectively. This indicates the presence of two distinct MgH_2 size distributions in the samples.

The measured TDS profiles are in good agreement with the Sieverts' measurements because sample X2-Mg has the fastest desorption rate at lower temperatures, while the difference is less pronounced at higher temperatures. The hydrogen desorption kinetics of MgH_2 can be improved and even tuned through confinement and variation of the texture parameters of the nanoporous scaffolds, which will be further explored in our future studies. Here, monoliths of RF-gel were infiltrated only one time with $MgBu_2$ heptane solution, giving a volumetric MgH_2 content of ~12 vol % in both samples (see Table 2). This suggests that the two porous aerogels X1 and X2 are completely loaded with crystalline $MgBu_2$. Furthermore, it indicates that the hydrogen storage capacity can be increased considerably by repeating the $MgBu_2$/heptan impregnation method and hydrogenation process several times.

In this study, the kinetic properties of magnesium hydride were clearly improved over several cycles of hydrogen release and uptake by nanoconfinement in aerogel with pore sizes of 7 and 22 nm. On the other hand, no thermodynamic improvements were observed, which is in accordance with theoretical studies suggesting that only pore sizes <2 nm may improve the thermodynamic properties of magnesium hydride.[20]

CONCLUSIONS

A new modified procedure for embedding MgH_2 nanoparticles into porous scaffold materials has been presented. Monoliths of RF-gels (0.4 cm^3) were infiltrated with excess $MgBu_2$ in heptan solution. The use of monoliths allows convenient removal of surface excess $MgBu_2$ mechanically and may increase the fraction of nanoconfined magnesium hydride in the composite material relative to surface excess MgH_2. The uptake of magnesium hydride was found to be proportional to the pore volume of the aerogel material, that is, giving a maximal volumetric MgH_2 content of ~12 vol % for one infiltration with $MgBu_2$ heptane solution. Sieverts' measurements revealed that ~81% of the loaded MgH_2 was accessible for reversible hydrogen storage. The hydrogen desorption kinetics of nanoconfined MgH_2 was influenced considerably by the pore size distribution of the scaffold material, and it was found that the smaller pores mediated faster desorption rate, possibly due to a size reduction of the confined hydride.

METHODS

Sample Preparation. The resorcinol formaldehyde aerogels, denoted RF-gels in the following, were prepared according to previously published procedures.[26,30] Sample X1 was prepared by mixing 10.361 g of resorcinol (Aldrich, 99%), 15.274 g of a 37 wt % formaldehyde in a water solution stabilized by ~10% methanol (Merck), 14.374 g of deionized water, and 0.032 g of Na_2CO_3 (Merck, 99.5%) in a beaker with continuous stirring. The organic fraction was 40 wt %, and the molar ratio of resorcinol/sodium carbonate was 312. Sample X2 was prepared by mixing 8.630 g of resorcinol, 12.893 g of 37 wt % formaldehyde in water stabilized by methanol, 5.1 g of deionized water, and 0.0464 g of Na_2CO_3 in a beaker with continuous stirring. The organic fraction was 50 wt %, and the molar ratio of resorcinol/sodium carbonate was 179. Both batches were stirred until a homogeneous solution was obtained. Afterward, each mixture was divided into several polypropylene bottles in order to keep the depth of the liquid phase below 0.5 cm. The polypropylene bottles were sealed with a lid, and the mixtures were initially aged at room temperature for 24 h and then heated to 50 °C for 24 h and to 90 °C for 72 h and afterward left to cool naturally in air. Monoliths of blackish solid gel were recovered and infiltrated with excess amounts of acetone. The acetone bath was displaced two times within a period of 3−4 days. The gels were left to dry in a fume hood for several days. Finally, the monolithic gels were cut into smaller pieces (*ca.* 0.4 cm^3) and pyrolyzed in a tube oven under a nitrogen flow, by heating to 800 °C (heating rate 2.6 °C/min) and dwelling for 6 h at 800 °C. The furnace was then turned off, and the samples were left there to cool naturally to room temperature.

A new modified procedure was developed in order to embed magnesium hydride in nanoporous scaffolds.[29] Selected gels were first activated at 400 °C in vacuum for several hours in order to remove moisture and gases from the porous structure. Afterward, monoliths of RF-gel (*ca.* 0.4 cm^3) were covered with excess amounts of a solution consisting of 1 M dibutylmagnesium, $MgBu_2$, in heptane (Aldrich), which also contains triethylaluminum. This infiltration procedure was performed under a purified argon atmosphere in a glovebox. The aerogels in $MgBu_2$ solution were left to dry for several days until the solvent heptane was fully evaporated and the dibutylmagnesium had crystallized in the pores. The monoliths of gels were easily distinguished and separated from the excess amount of dibutylmagnesium. White crystalline dibutylmagnesium deposited onto the surface of the rigid aerogel material was carefully removed mechanically. The uptake of magnesium in the gels was calculated by measuring the mass of the aerogels before and after loading them with $MgBu_2$ (see Table 2). Dibutylmagnesium reacts with hydrogen to form magnesium hydride and butane at a temperature of 170 °C and a hydrogen pressure of 50 bar.[29] This reaction was carried out under inert conditions in either a PCTpro 2000 apparatus from Hy-energy[34] or a custom-made Sieverts' apparatus[35] by applying a hydrogen pressure of 50−78 bar and heating to temperatures in the range of 170−200 °C. A sample of magnesium hydride was prepared by hydrogenation of crystalline dibutylmagnesium (without aerogel) using the same procedure as described above. This sample is denoted AM and was used as a reference. Commercially available micrometer-sized MgH_2 powder (ABCR, 98%), denoted BM, was also used for reference.

Aerogel Characterization. Characterization of the nanoporous aerogel scaffold material was performed by gas adsorption and desorption using a Nova 2200e surface area and pore size analyzer from quantachrome. The aerogels were degassed under vacuum for several hours at 300 to 320 °C, prior to the measurements. A full absorption and desorption isotherm was measured in the pressure range 0 to 1 p/p_0 at liquid nitrogen temperatures with nitrogen gas as the adsorbent. Data were analyzed using the *t*-plot method,[36,37] the Brunner−Emmet−Teller (BET) method,[38] and the Barrett−Joyner−Halenda (BJH) method, and the total volume was calculated from a single point at $p/p_0 \sim 1$.[39]

Characterization of the Hydrogen Storage Properties for Nanoconfined MgH_2. The cyclic stability of MgH_2 embedded in aerogel was studied by Sieverts' measurements (PCTpro 2000),[34] and a total of four hydrogen uptake and release cycles were performed. Monoliths of aerogel (~0.4 cm^3) loaded with crystalline dibutylmagnesium corresponding to 30−82 mg of magnesium were transferred to an autoclave and sealed under argon in a glovebox. The autoclave was attached to the PCTpro 2000 apparatus, and the synthesis of MgH_2 was performed under similar conditions as described above. Hydrogen desorption data were collected in the temperature range of room temperature to 380 °C, and with the temperature kept fixed at 250, 300, and 380 °C for 5, 5, and 6 h. The heating rate was 2 °C/min. Hydrogen absorption was performed at $p(H_2) \sim 100$ bar in the temperature range of 300 to 380 °C for several hours.

Characterization of the hydrogen desorption kinetics of the first desorption cycle was also performed by thermal desorption spectroscopy (TDS) using an apparatus described elsewhere.[40,41] Prior to the measurements, the synthesis of MgH_2 from crystalline $MgBu_2$ was performed according to the procedure described above. Samples corresponding to 1−5 mg of MgH_2 were placed in a high vacuum system connected to a turbo molecular pump with a constant pumping rate at pressures between 10^{-9} and 10^{-2} Torr. The sample was heated to a temperature of 700 °C with a heating rate of 3.6 °C/min, and the hydrogen desorbed from the sample was detected by a computer-controlled mass spectrometer measuring $m/e < 20$. Pristine aerogel samples were pretreated and analyzed by Sieverts' apparatus and TDS under the same conditions as described above for MgH_2-loaded samples.

Scanning electron microscopic (SEM) images and energy-dispersive spectrometry measurements (EDS) were acquired in a combined setup by means of a Nova NanoSEM 600 from FEI equipped with an EDS detector. Monoliths of RF-gel cycled with hydrogen release and uptake six times in the PCTpro were crushed into smaller units, and fragments from the center of the gels were selected in order to study the interior of the monoliths. The samples were mounted on carbon tape supported by an aluminum sample holder. This procedure was performed under atmospheric conditions, and magnesium was expected to be oxidized by moistures and oxygen to form magnesium oxide. EDS diagrams were obtained by applying a voltage of 8 kV and collecting the Kα signals. EDS maps were acquired by selectively measuring the magnesium Kα signal. *In situ* synchrotron radiation powder X-ray diffraction (SR-PXD) data were collected at

beamline I911 at MAX-lab, Lund, Sweden. Fragments of the interior of $MgBu_2$ loaded RF-aerogel monoliths were crushed and placed in a sapphire capillary tube. The tube containing *ca.* 10 mm of powder was mounted in an airtight sample holder. The sample holder was moved from the glovebox to the diffractometer under inert conditions. The selected X-ray wavelength was $\lambda = 0.9077$ Å, the X-ray exposure time was 30 s, and *in situ* SR-PXD data were collected using a MAR CCD detector. The sample was heated in the temperature range from room temperature to 350 °C with a heating rate of 7.5 °C, and the hydrogen pressure was $p(H_2) \sim 50$ bar. The synthesis of MgH_2 from dibutylmagnesium, sample AM, was also investigated in the temperature range from room temperature to 170 °C (heating rate 7.5 °C/min) and a hydrogen pressure of $p(H_2) = 50$ bar.

Acknowledgment. We are grateful to the Danish National Research Council under the program DanScatt for financial support. Partial funding by the European Commission DG Research (Contract SES6-2006-518271/NESSHY) is gratefully acknowledged by some of the authors.

Supporting Information Available: Scanning electron microscopic (SEM) images and energy-dispersive spectrometry (EDS) measurements of samples X1-Mg and X2-Mg. This material is available free of charge *via* the Internet at http://pubs.acs.org.

REFERENCES AND NOTES

1. Schlapbach, L.; Züttel, A. Hydrogen-Storage Materials for Mobile Applications. *Nature* **2001**, *414*, 353–358.
2. Ritter, J. A.; Ebner, A. D.; Wang, J.; Zidan, R. Implementing a Hydrogen Economy. *Mater. Today* **2003**, *6*, 18–23.
3. Grochala, W.; Edwards, P. P. Thermal Decomposition of the Non-Interstitial Hydrides for the Storage and Production of Hydrogen. *Chem. Rev.* **2004**, *104*, 1283–1315.
4. Orimo, S.; Nakamori, Y.; Eliseo, J. R.; Züttel, A.; Jensen, C. M. Complex Hydrides for Hydrogen Storage. *Chem. Rev.* **2007**, *107*, 4111–4132.
5. Felderhoff, M.; Weidenthaler, C.; von Helmolt, R.; Eberle, U. Hydrogen Storage: The Remaining Scientific and Technological Challenges. *Phys. Chem. Chem. Phys.* **2007**, *9*, 2643–2653.
6. Dornheim, M.; Eigen, N.; Barkhordarian, G.; Klassen, T.; Bormann, R. Tailoring Hydrogen Storage Materials towards Application. *Adv. Eng. Mater.* **2006**, *8*, 377–385.
7. Zaluska, A.; Zaluski, L.; Ström-Olsen, J. O. Nanocrystalline Magnesium for Hydrogen Storage. *J. Alloys Compd.* **1999**, *289*, 217–225.
8. XiangDong, Y.; GaoQing, L. Magnesium-Based Materials for Hydrogen Storage: Recent Advances and Future Perspectives. *Chin. Sci. Bull.* **2008**, *53*, 2421–2431.
9. Asukama, Y.; Miyauchi, S.; Yamamoto, T.; Aoki, H.; Miura, T. Numerical Analysis of Absorbing and Desorbing Mechanism for the Metal Hydride by Homogenization Method. *Int. J. Hydrogen Energy* **2003**, *28*, 529–536.
10. Vigeholm, B.; Jensen, K.; Larsen, B.; Pedersen, A. S. Elements of Hydride Formation Mechanisms in Nearly Spherical Magnesium Powder Particles. *J. Less-Common Met.* **1987**, *131*, 133–141.
11. Vigeholm, B.; Kjøller, J.; Larsen, B.; Pedersen, A. S. Formation and Decomposition of Magnesium Hydride. *J. Less-Common Met.* **1983**, *89*, 135–144.
12. Bérube, V.; Radtke, G.; Desselhaus, M.; Chen, G. Size Effects on the Hydrogen Storage Properties of Nanostructured Metal Hydrides: A Review. *Int. J. Energy Res.* **2007**, *31*, 637–663.
13. Vajo, J. J.; Salguero, T. T.; Gross, A. F.; Skeith, L. S.; Olson, G. L. Thermodynamic Destabilization and Reaction Kinetics in Light Metal Hydride Systems. *J. Alloys Compd.* **2007**, *446*−*447*, 409–414.
14. Yao, X.; Zhu, Z. H.; Cheng, H. M.; Lu, G. Q. Hydrogen Diffusion and Effect on Grain Size on Hydrogenation Kinetics in Magnesium Hydrides. *J. Mater. Res.* **2008**, *23*, 336–340.
15. Zaluski, L.; Zaluska, A.; Ström-Olsen, J. O. Nanocrystalline Metal Hydrides. *J. Alloys Compd.* **1997**, *253*−*254*, 70–79.
16. Kirchheim, R.; Mütschele, T.; Kieninger, W.; Gleiter, H.; Birringer, R.; Koblé, T. D. Hydrogen in Amorphous and Nanocrystalline Metals. *Mater. Sci. Eng.* **1988**, *99*, 457–462.
17. Cheung, S.; Deng, W. Q.; Duin, A. C. T.; Goddard, W. A. Reactive Force Field for Magnesium Hydride Systems. *J. Phys. Chem. A* **2005**, *109*, 851–859.
18. Liang, J. J. Theoretical Insight on Tailoring Energetics of Mg Hydrogen Absorption/Desorption through Nano-Engineering. *Appl. Phys. A: Mater. Sci. Process.* **2005**, *80*, 173–178.
19. Berube, V.; Chen, G.; Dresselhaus, M. S. Impact of Nanostructuring on the Enthalpy of Formation of Metal Hydrides. *Int. J. Hydrogen Energy* **2008**, *33*, 4122–4131.
20. Wagemans, R. W. P.; Lenthe, J. H.; de Jongh, P. E.; Dillen., A. J.; Jong., K. P. Hydrogen Storage in Magnesium Clusters: Quantum Chemical Study. *J. Am. Chem. Soc.* **2005**, *127*, 16675–16680.
21. Berlouis, L. E. A.; Cabrera, E.; Hall-Barientos, E.; Hall, P. J.; Dodd, S. B.; Morris, D.; Imam, M. A. Thermal Analysis Investigation of Hydriding Properties of Nanocrystalline Mg-Ni and Mg-Fe-Based Alloys Prepared by High-Energy Ball Milling. *J. Alloys Compd.* **2000**, *305*, 82–89.
22. Gertsman, V. Y.; Birringer, B. On the Room-Temperature Grain Growth in Nanocrystalline Copper. *Scr. Metall. Mater.* **1994**, *30*, 577–581.
23. Vigeholm, B.; Kjøller, J.; Larsen, B.; Pedersen, A. S. Hydrogen Sorption Performance of Pure Magnesium during Continued Cycling. *Int. J. Hydrogen Energy* **1983**, *8*, 809–817.
24. Gutowska, A.; Li, L.; Shin, Y.; Wang, M. C.; Li, S. X.; Linehan, J. C.; Smith, R. S.; Kay, B. D.; Schmid, B.; Shaw, W.; Gutowski, M.; Autrey, T. Nanoscaffold Mediates Hydrogen Release and the Reactivity of Ammonia Borane. *Angew. Chem., Int. Ed.* **2005**, *44*, 3578–3582.
25. Schüth, F.; Bogdanovic, B.; Taguchi, A. Patent Application WO2005014469, July, 2003.
26. Gross, A. F.; Vajo, J. J.; Atta, S. L. V.; Olson, G. L. Enhanced Hydrogen Storage Kinetics of $LiBH_4$ in Nanoporous Carbon Scaffolds. *J. Phys. Chem. C* **2008**, *112*, 5651–5657.
27. de Jongh, P. E.; Wagemans, R. W. P.; Eggenhuisen, M. T.; Dauvillier, B. S.; Radstake, P. B.; Meeldijk, J. D.; Geus, J. W.; Jong, K. P. The Preparation of Carbon-Supported Magnesium Nanoparticles Using Melt Infiltration. *Chem. Mater.* **2007**, *19*, 6052–6057.
28. Gross, A. F.; Ahn, C. C.; Atta, S. L. V.; Liu, P.; Vajo, J. J. Fabrication and Hydrogen Sorption Behavior of Nanoparticulate MgH_2 Incorporated in Porous Carbon Host. *Nanotechnology* **2009**, *20*, 204005.
29. Zhang, S.; Gross, A. F.; Atta, S. L. V.; Lopez, M.; Liu, P.; Ahn, C. C.; Vajo, J. J.; Jensen, C. M. The Synthesis and Hydrogen Storage Properties of a MgH_2 Incorporated Carbon Aerogel Scaffold. *Nanotechnology* **2009**, *20*, 204027.
30. Li, W. C.; Lu, A. H.; Weidenthaler, C.; Schüth, F. Hard-Templating Pathway To Create Mesoporous Magnesium Oxide. *Chem. Mater.* **2004**, *16*, 5676–5681.
31. Al-Muthaseb, S. A.; Ritter, J. A. Preparation and Properties of Resorcinol-Formaldehyde Organic and Carbon Gels. *Adv. Mater.* **2003**, *15*, 101–114.
32. Li, J.; Wang, X.; Huang, Q.; Gamboa, S.; Sebastian, P. J. Studies on Preparation and Performances of Carbon Aerogel Electrodes for the Application of Supercapacitor. *J. Power Sources* **2006**, *158*, 784–788.
33. Andreasen, A.; Sørensen, M. B.; Burkarl, R.; Møller, B.; Molenbrok., A. M.; Pedersen, A. S.; Andreasen, J. W.; Nielsen, M. M.; Jensen, T. R. Interaction of Hydrogen with an Mg-Al Alloy. *J. Alloys Compd.* **2005**, *404*−*406*, 323–326.
34. www1.eere.energy.gov/hydrogenandfuelcells/pdfs/bestpractices_ h2_storage_materials.pdf; http://www.setaram.com/PCTPro-2000.htm.
35. Panella, B.; Hirscher, M.; Roth, S. Hydrogen Adsorption in Different Carbon Nanostructures. *Carbon* **2005**, *43*, 2209–2214.
36. Halsey, G. Physical Adsorption on Non-Uniform Surfaces. *J. Chem. Phys.* **1948**, *16*, 931–937.

37. de Boer, J. H.; Linsen, B. G.; Plas, Th.; Zondervan, G. J. Studies on Pore Systems in Catalysts VII. Description of the Pore Dimensions of Carbon Blacks by the *t* Method. *J. Catal.* **1969**, *4*, 649.
38. Brunauer, S.; Emmet, P.; Teller, E. Adsorption of Gases in Multimolecular Layers. *J. Am. Chem. Soc.* **1939**, *60*, 309–319.
39. Barrett, E. P.; Joyner, L. G.; Halenda, P. P. The Determination of Pore Volume and Area Distributions in Porous Substances. I. Computations From Nitrogen Isotherms. *J. Am. Chem. Soc.* **1951**, *73*, 373–380.
40. Mommer, N.; Hirscher, M.; Cuevas, F.; Kronmüller, H. Influence of the Microstructure on the Desorption Kinetics of Single- and Multiphase LaNiFe Alloys. *J. Alloys Compd.* **1998**, *266*, 255–259.
41. von Zeppelin, F.; Haluska, M.; Hirscher, M. Thermal Desorption Spectroscopy as a Quantitative Tool To Determine the Hydrogen Content in Solids. *Thermochim. Acta* **2003**, *404*, 251–258.